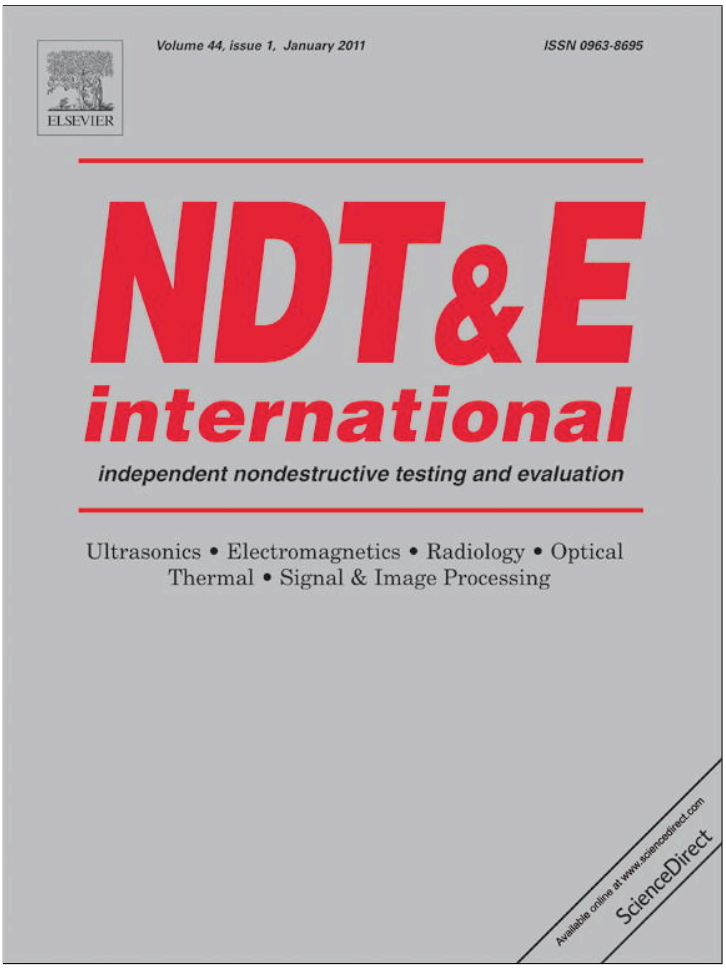

NDT&E International 44 (2011) 21–31

Contents lists available at ScienceDirect

NDT&E International

journal homepage: www.elsevier.com/locate/ndteint

Elastic-wave modulation approach to crack detection: Comparison of conventional modulation and higher-order interactions

V.Yu. Zaitsev *, L.A. Matveev, A.L. Matveyev

Institute of Applied Physics RAS, Uljanova Str., 46, Nihny Novgorod, 603950, Russia

ARTICLE INFO

Article history:
Received 4 November 2009
Received in revised form
1 September 2010
Accepted 3 September 2010
Available online 16 September 2010

Keywords:
Nonlinear acoustic diagnostics
Crack detection
Wave modulation spectroscopy

ABSTRACT

Comparison of recent theoretical estimates with experiments has indicated that the ultimate sensitivity of the conventional modulation technique of crack detection is mainly determined by the background modulation produced by the quadratic component of the atomic nonlinearity of the matrix material. Much smaller level of masking nonlinear effects is typical of higher-order interactions due to cubic and higher-order components in the power-series expansion of the background nonlinearity of the solid. In contrast, the level of formally higher-order components originated due to nonlinearity of crack-like defects can be comparable with that of the first-order components. Such strongly increased efficiency of higher-order interactions is due to the fact that crack-like defects often demonstrate non-analytic (non power-law) nonlinearity even for moderate acoustic amplitudes. Besides the increased level, the higher-order components arisen due to non-analytic nonlinearity of cracks can demonstrate significantly different functional behavior compared to manifestations of the atomic nonlinearity. This difference can also help to discriminate the contributions of the defects and the background atomic nonlinearity. Here, we focus on the main differences between the modulation components arisen due to cubic terms in the power-series expansion of the atomic nonlinearity and similar components generated by clapping Hertzian nonlinearity of inner contacts in cracks. We also examine experimental examples of higher-order modulation interactions in damaged samples. These examples clearly indicate non-analytical character of the defects' nonlinearity and demonstrate that the use of higher-order modulation effects can significantly improve the ultimate sensitivity and reliability of the modulation approach to detection of crack-like defects.

1. Introduction

High interest to the nonlinear-modulation acoustic method of crack detection is significantly motivated by expectations to achieve superior detection sensitivity compared to other methods of nondestructive testing [1–10]. To ensure this goal, the main attention in the development of the nonlinear-modulation technique is usually paid to the reduction of various technical nonlinearities, whereas the masking effect of the atomic nonlinearity of the intact material is neglected. Apparently, this view is supported by the notion that the dimensionless quadratic nonlinear parameter β for homogeneous solids is on the order of 10^0 [11,12]. Therefore, for typical acoustic strains $\varepsilon \leq 10^{-5}$, the corresponding nonlinear correction $\beta\varepsilon$ should have the relative level about -100 to -80 dB, which is indeed practically negligible. Furthermore, contributions of terms higher than quadratic seem to be beyond reasonable measurable values.

It has recently been argued [13] that under resonant conditions, such simplest quasistatic arguments can drastically underestimate the modulation level due to the atomic nonlinearity. More accurate resonant estimates of conventionally measured modulation components $\omega \pm \Omega$ (where ω and Ω are the frequencies of the interacting weak probe and the intense pump waves, respectively) indicate that the contribution of technical nonlinearities of the modern equipment can be equal to or even less than the contribution of the quadratic atomic nonlinearity. Therefore, the atomic nonlinearity becomes the main factor, which limits the ultimate sensitivity of the conventional nonlinear-modulation approach. If the difference between the levels of the $\omega \pm \Omega$ sidelobes for the studied samples is comparable with the natural variability of the background modulation (typically, 10–15 dB and even more [13]), it can be attributed to many factors other than the sample damage, which complicates the early detection of cracks.

As a natural way to improve the sensitivity and reliability of the nonlinear-modulation approach to crack detection, the possibility to intentionally use higher-order nonlinear interactions was mentioned in Ref. [13]. Indeed, for higher-order

* Corresponding author.
E-mail addresses: vyuzai@hydro.appl.sci-nnov.ru, vyuzai@mail.ru (V.Yu. Zaitsev).

0963-8695/$ - see front matter © 2010 Elsevier Ltd. All rights reserved.
doi:10.1016/j.ndteint.2010.09.002

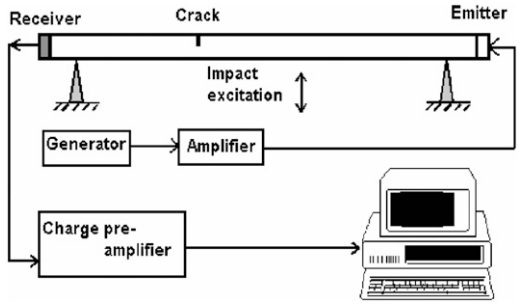

Fig. 1. Schematically shown configuration of nonlinear-modulation experiments [13–15] with sinusoidal probe wave at frequency ω tuned in the range 50–70 kHz and impact-excited intense eigenmodes with frequencies Ω_i typically ranged from a few hundreds Hz to a few kHz.

interactions, one can expect a drastic decrease in the masking signal caused by the atomic nonlinearity for which the power-series law is typical, such that each additional order in strain ensures ~80–100 dB additional reduction of the masking components due to the atomic nonlinearity. In contrast, the nonlinearity of cracks can significantly differ from the power-law type even for moderate acoustic amplitudes, so that the level of higher-order and lower-order modulational components induced by crack-like defects can be comparable. Therefore, one may expect that the observation of higher-order modulational interactions can significantly enhance the contrast between intact and crack-containing samples.

In what follows, we discuss in more detail this idea and make comparison with the same series of experiments as discussed in Refs. [13–15]. We recall that in those measurements (for which the experimental configuration is schematically shown in Fig. 1), favorable conditions for multi-wave interactions were ensured by the impact excitation of a significant number of intense ("pump") low-number resonant eigenmodes of the sample at frequencies Ω_i. Initially, those measurements were processed according to the conventional nonlinear-modulation approach by singling out the quadratic-type modulational components $\omega \pm \Omega_i$ in the vicinity of the fundamental frequency $\omega \gg \Omega_i$ of a sinusoidal probe ultrasound wave. By re-processing the experimental records, we demonstrate that more complex components of the $\omega \pm \Omega_i \pm \Omega_j$ type can also be well observed. In what follows, we call them "cascade components" (instead of "higher-order") to avoid the incorrect impression that their amplitude is of the next order of smallness in comparison with the conventionally discussed $\omega \pm \Omega_i$ modulation sidelobes. We show that the cascade components can ensure noticeably higher contrast between the reference and crack-containing samples. We also show that the amplitude dependences for the cascade components $\omega \pm \Omega_i \pm \Omega_j$ (i.e., formally cubic type) significantly differ from the scaling law expected for classical cubic nonlinearity, which can be used as an additional signature of the presence of crack-like defects. We demonstrate that the actual amplitude behavior of the cascade components can be fairly well modeled by clapping nonlinearity of inner Hertzian contacts in cracks.

2. Preliminary note on indications of clapping Hertzian nonlinearity in acoustically driven crack-like defects

For the further discussion, it is essential to recall that high softness of crack-like defects results in high increase of the local strain, which is the physical reason of the strongly increased nonlinearity of damaged samples. It can readily be shown that in the expansion of the defect's equation of state in a power-series in strain, the nonlinear terms of nth order increase as $1/\varsigma^{n-1}$, where $\varsigma \ll 1$ is the small parameter describing the defect softness compared to the surrounding intact solid [16,17]. Formally this means that for strains $\varepsilon \sim \varsigma$, the higher-order nonlinear terms should be of the same order as the lower-order terms. Actually, however, the power-series expansion is no more valid for such oscillation amplitudes, and the regime of the defect deformation becomes essentially non-analytical, so that nonlinear components of formally different orders can have amplitudes of the same order of smallness. For example, if Hertzian contacts at the crack interface begin to clap, then their nonlinearity can be approximated as $\varepsilon^{3/2}H(\varepsilon)$ (where strain ε is considered positive for compression and $H(\varepsilon)$ is a Heaviside function). Consequently, amplitudes of all higher harmonics produced by such nonlinearity under sinusoidal excitation $\varepsilon = A\cos(t)$ exhibit the same functional dependence $\propto A^{3/2}$, which is easily seen by taking the Fourier transform of $\varepsilon^{3/2}H(\varepsilon)$.

Due to high softness of crack-like defects, such a non-analytical clapping regime for inner contacts can occur for fairly moderate average acoustic strains, e.g., on the order of $\sim 10^{-5}$ and even less. Fig. 2 shows experimental examples of amplitude dependences of the 2nd, 3rd, and 4th harmonics in a sinusoidally excited resonant sample containing an artificial crack-like defect. The same power-law behavior with the exponent 3/2 for all harmonics (see the slopes of the solid lines) corresponds to the clapping Hertzian nonlinearity. The sample excited near its first resonance represented a glass rod (1 cm in diameter and about 20 cm in length) with one free and another acoustically rigid (due to cemented massive backload) boundary. Like in Ref. [18], the defect was modeled by a transversal diamond-saw-cut (1 mm in width and 4–5 mm in depth) in which a small metal plate was inserted. By slightly changing the plate position it was possible to observe different nonlinear regimes of the defect oscillations, including the contact-clapping regime, which could be attained at fairly moderate strains of 10^{-6}–10^{-5}. For the classical power-law nonlinearity, the higher harmonics should exhibit the quadratic, cubic, fourth-power, etc. dependences with pronouncedly different slopes in log–log scale. Certainly, the relative levels of the harmonics in Fig. 2 are affected by resonant properties of the sample, so that the resonant odd-type 3rd harmonic is higher than the non-resonant 2nd and 4th ones. When the inset was removed (which corresponded to the disappearance of the

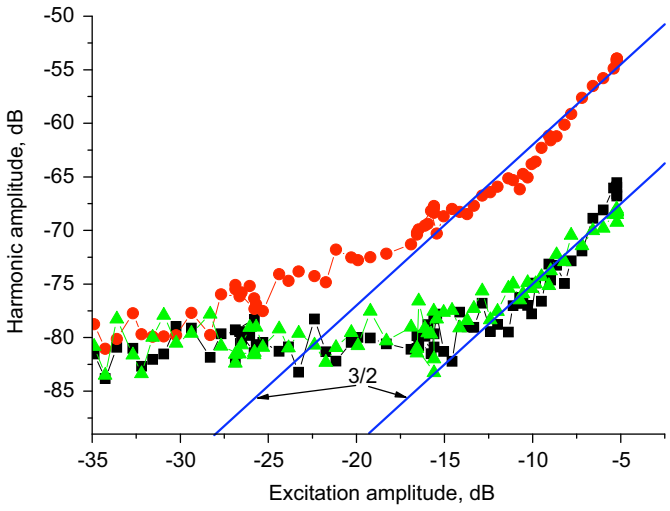

Fig. 2. Amplitudes of the 2nd (squares), 3rd (circles), and 4th (triangles) harmonics in a rod-shape resonant sample with an artificial crack-like defect as functions of the fundamental-harmonic amplitude. The maximal strain of the harmonic excitation in the defect vicinity was 5×10^{-6}.

crack-like defect), all harmonics were hardly noticeable against the measurement noise.

Returning to the discussed nonlinear-modulation experiments [13–15] with multi-frequency pump components Ω_i, Ω_j, etc., instead of different higher harmonics we compare the conventional modulation sidelobes $\omega \pm \Omega_{i,j}$ and cascade components $\omega \pm \Omega_i \pm \Omega_j$, which formally correspond to the second- and third-order nonlinear interactions, respectively. Thus for a power-series law typical of pure atomic nonlinearity, cubic components $\omega \pm \Omega_i \pm \Omega_j$ should have practically immeasurable level (80–100 dB lower than the quadratic $\omega \pm \Omega_{i,j}$ components).

Examples of modulation spectra observed in the experiments [13–15] for defect-containing and reference samples (a railway-wheel axle and disk) are shown in Fig. 3, where conventional $\omega \pm \Omega_{i,j}$ components are plotted in black dashed lines and cascade components $\omega \pm \Omega_i \pm \Omega_j$ are shown in a lighter color (solid lines). The expected positions of the sidelobes were calculated using the experimentally measured frequencies of the impact-excited pump eigenmodes in the lower-frequency part of the spectrum. The expected and actual frequencies of the sidelobes were considered coinciding within the double frequency resolution determined by the inverse width of the used time window. Typically its value was 0.2 s, which corresponded to 5 Hz spectral resolution. The width of the time window was intentionally limited to ensure the observation of the time dependences of different spectral components within the characteristic decay time (typically 0.8–1.0 s) of the impact-excited eigenmodes that produced the modulation of the sinusoidal probe wave. To ensure a stabler form of the modulation spectrum, the probe-wave frequency was tuned in the range 50–70 kHz typically in steps of 500 Hz and at each step identical impacts excited the pump eigenmodes. The spectra in Fig. 3 are averaged over 10–15 steps and correspond to the middle of the entire time window of the observation. The probe-wave component is not explicitly shown: its amplitude is normalized to zero dB and its position on the frequency axis is shifted to zero frequency for each measurement step.

For an ideally linear measurement system (assuming that the background modulation was entirely produced by the atomic nonlinearity), the cascade components would not be visible at all in the scale of Fig. 3. The actual noticeable level of cascade components in the reference samples is evidently explained by the parasite nonlinearity of the measurement system. Nevertheless, in Fig. 3, the visual contrast between the reference and damaged samples is significantly higher for the cascade components $\omega \pm \Omega_i \pm \Omega_j$ than for the conventional $\omega \pm \Omega_{i,j}$ modulation sidelobes.

To better quantify the difference between the spectra shown in Fig. 3 for the reference and damaged samples we use a histogram representation by analogy with Ref. [19]. Figs. 4 and 5 show the histograms in which the vertical axis corresponds to the summed energy for either conventional or cascade sidelobes whose amplitudes fall into certain amplitude range corresponding to the width of individual bins on the horizontal axis (in Figs. 4 and 5 the bin width is equal to 4 dB, although the exact value is not critical). Fig. 4 corresponds to the spectra shown in Fig. 3a and b obtained for the disks and Fig. 5 is for the spectra Fig. 3a′ and b′ obtained for the axle with an artificial crack-like defect and without it. The right panels in Fig. 4 demonstrate that the energies of conventionally considered $\omega \pm \Omega_{i,j}$ modulation sidelobes for the reference and defect-containing samples do not change drastically (since the extent of damage is intentionally chosen not very high). Their total energies of the $\omega \pm \Omega_{i,j}$ sidelobes summed over all bins differ by 5 dB only. Therefore, such conventionally used components do not allow one to make a reliable conclusion

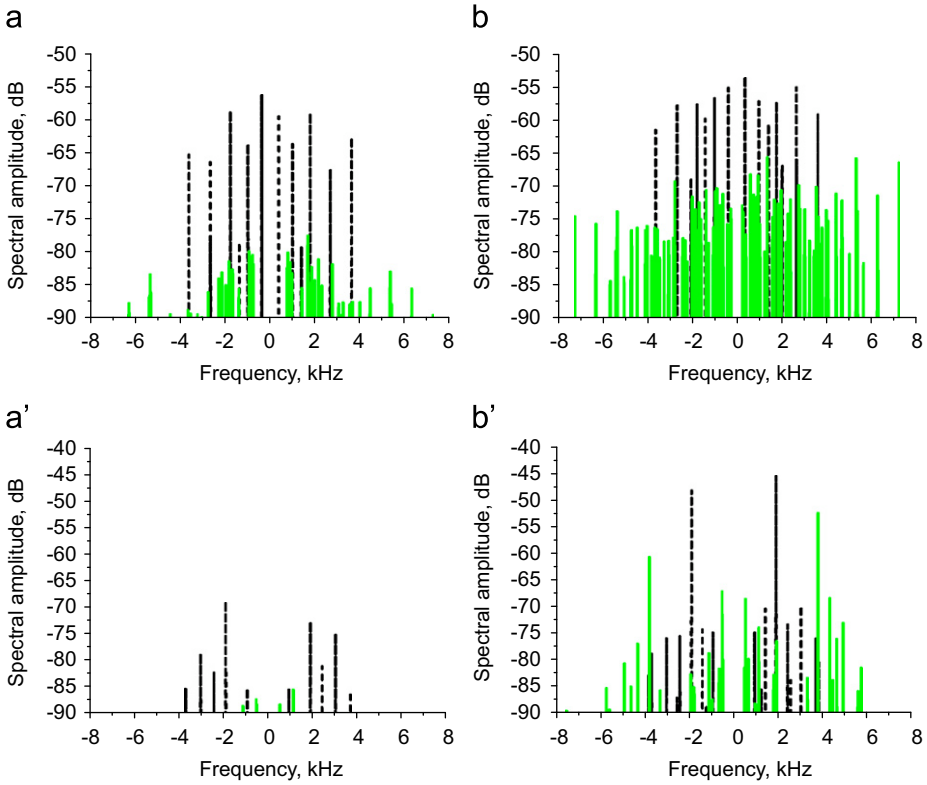

Fig. 3. Examples of normalized averaged modulation spectra for the samples without defects (panels (a) and (a′)) and with a defect ((b) and (b′)). The upper row is for railway-wheel disks (the defect-containing disk has naturally developed fatigue damage). The lower row is for a railway-wheel axle (in which an artificial crack-like defect could be created by inserting a small steel plate in the saw-cut 7 mm in depth). Black dashed lines correspond to conventional modulation components $\omega \pm \Omega_{i,j}$, and lighter solid lines are for the cascade components $\omega \pm (\Omega_i \pm \Omega_j)$.

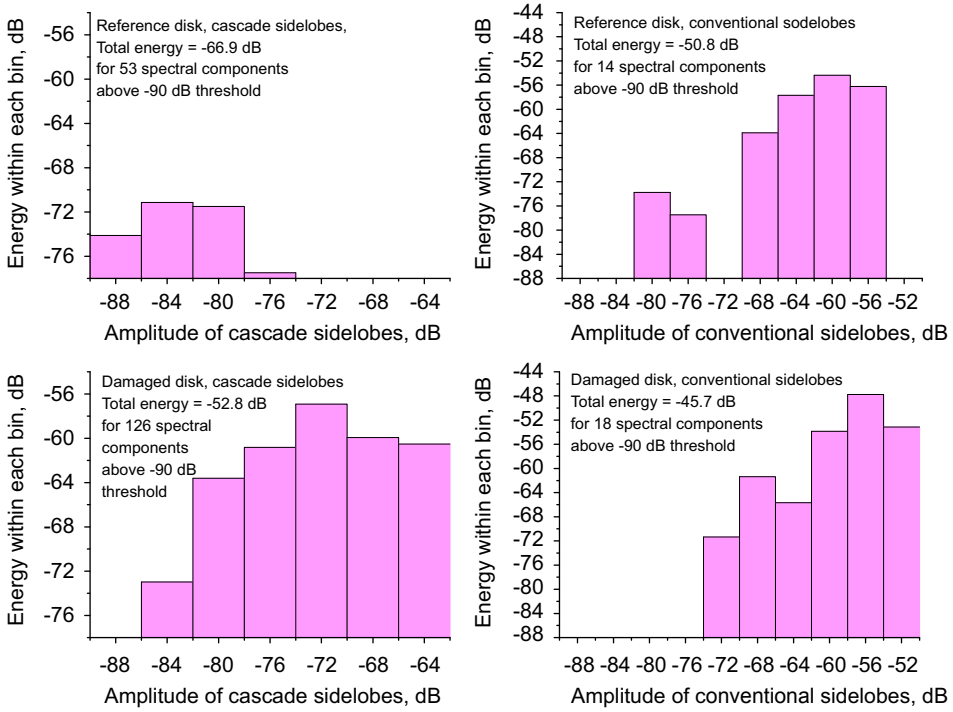

Fig. 4. Histograms of the energy distribution for the conventional (right panels) and cascade (left panels) sidelobes. Upper and lower rows are for the reference and damaged disks, respectively (the same samples as for panels Fig. 3(a) and (b)).

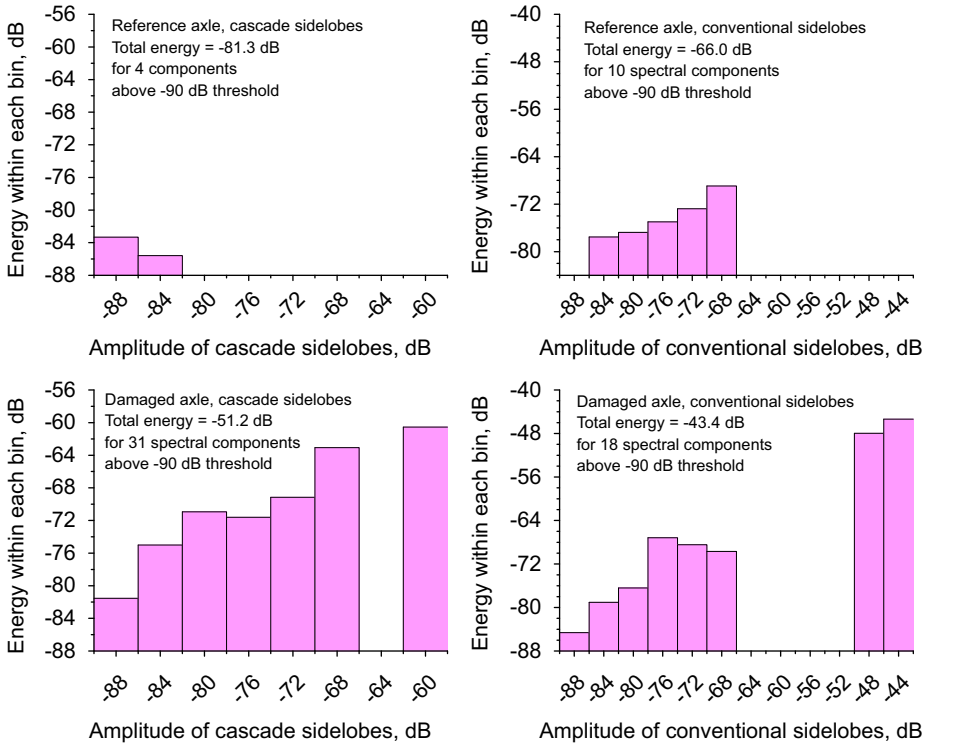

Fig. 5. Histograms of the energy distribution for the conventional (right panels) and cascade (left panels) sidelobes. Upper and lower rows are for the reference and crack-containing axles, respectively (the same samples as for panels Fig. 3(a′) and (b′)).

whether the defect is present or not. The panels in the left columns in Fig. 4 correspond to the cascade components $\omega \pm \Omega_i \pm \Omega_j$, whose energy demonstrate significantly higher contrast between the reference and damaged samples (over 14 dB for the summed energies).

In Fig. 5 for the axles, the contrast between the cascade $\omega \pm \Omega_i \pm \Omega_j$ sidelobes is even more impressive (over 30 dB in the summed energies), although for the conventionally used sidelobes $\omega \pm \Omega_{i,j}$, the contrast is also better than in Fig. 4 (22.5 dB in the summed energies). However, it is evident from both the

histograms in Fig. 5 and the spectral plot in Fig. 3b′ that this better contrast is due to the only pair of the most intense $\omega \pm \Omega_j$ sidelobes around ± 1.9 kHz, for generation of which the position of the crack happened to be especially favorable. If we exclude such exceptional sidelobes from the considered $\omega \pm \Omega_{i,j}$ components as well as the related $\omega \pm \Omega_i \pm \Omega_j$ cascade sidelobes at the double frequency ± 3.8 kHz, then the contrast for summed energy of the retained $\omega \pm \Omega_{i,j}$ components becomes very weak (only 2.8 dB), whereas for the retained cascade $\omega \pm \Omega_i \pm \Omega_j$ components it remains quite high (21.3 dB).

Thus in Figs. 4 and 5, the contrast in the energies for the cascade $\omega \pm \Omega_i \pm \Omega_j$ components (as well as in their numbers) is significantly more pronounced. However, one should bear in mind that for such a comparison, a similar reference sample is necessary for which the reference spectrum should be obtained under virtually identical experimental conditions: the same nonlinearity of the measurement system, similar boundary conditions, and similar excitation amplitudes, since even under other identical conditions, the efficiency of nonlinear interactions significantly depends of the interacting-wave amplitudes. Therefore, it is very desirable to have more robust (in the ideal case, independent of wave amplitudes) characteristics of the sample nonlinearity rather than the straightforward comparison with a reference sample under as similar experimental configuration as possible.

3. Normalized cumulative coefficients for the conventional (quadratic-type) and cascade modulation sidelobes

It was discussed in detail in Ref, [13] that the level of conventional modulation can noticeably (up to 20–30 dB) vary due to different interaction conditions for different modes. Therefore, to obtain stabler results, averaging over a number of pump- and probe-wave frequencies is required as well as a normalization procedure to exclude the direct influence of the pump-wave amplitudes on the modulation level. To quantify the average level of conventional (i.e., quadratic-type) modulational components in the case of multiple pump waves, the following normalized cumulative coefficient was used in Ref. [14]:

$$K_2 = \sqrt{\sum_i (V_+^2(i) + V_-^2(i))} \Big/ \left(\sqrt{\sum_i V_{pm}^2(i)} V_p \right), \tag{1}$$

where the summation is performed over the index i of the excited pump modes. Physically, the structure of this coefficient means that the energies $V_\pm^2(i)$ of all left- and right- modulation sidelobes are summed up. Then the square root of this energy (i.e., the averaged modulation-sidelobe amplitude) is divided by the amplitude V_p of the probe wave and by the square root of energies $V_{pm}^2(i)$ of the modulating pump modes. In the case of only one pump mode with index i, the denominator reduces to the product $V_{pm}(i)V_p$, and in the numerator, only sidelobes $V_\pm(i)$ produced by the ith pump mode are left. For the discussed multimode situation, the numerator is dominated by the most intense modulation sidelobes, whereas the most intense pump modes dominate the denominator. Since the sidelobe amplitudes strongly depend on the position of the crack with respect to the pump-mode structures, the summation over multiple pump modes diminishes the variance of K_2. Besides, this variance can further be decreased by averaging over the probe-wave frequency swept in a sufficiently wide range. It is also seen from Eq. (1) that the value of K_2 should depend on the amplification coefficients in the receiving equipment, which means that only the relative values of K_2 (i.e., comparison between the reference and studied samples under similar conditions) is physically meaningful. It is also clear that for a quadratic nonlinearity (for which the sidelobe amplitudes $V_\pm(i) \propto V_{pm}(i)V_p$), the value of coefficient K_2 should remain approximately constant as a function of the pump-wave amplitude. Indeed, in the experiments discussed in Refs. [13–15], the amplitudes of impact-excited pump waves decayed (by 10–50 dB for different modes) on the time intervals of the order of one second, whereas the current value of coefficient K_2 remained fairly stable (within several dB). This leads to the conclusion that the nonlinearity of the studied defects could reasonably be approximated by a quadratic function.

At first glance it seems that physically it is more reasonable to use individual normalization $[V_+^2(i) + V_-^2(i)]^{1/2}/[V_{pm}(i)V_p]$ for each triplet associated with the ith pump mode and then to average over the probe-wave frequency the individual coefficients. However, it was found that such individual coefficients are too unstable in practice. For instance, for some pump modes which were not longitudinal, the accelerometer aligned with the sample axis registered apparently very weak amplitudes. Therefore, those modes gave huge individual nonlinear coefficients, although the actual level of the resultant sidelobes and the strain in such modes were comparable with those for other modes. In other cases, eventual electrically induced signals could also produce strong fake sidelobes and the respective high individual coefficients. Therefore, somewhat rude, but much stabler cumulative coefficient (1) was chosen in Ref. [15].

For the cascade modulation components, in view of the larger number of interacting and resultant modes, the situation is even more complex. Under the simplest assumption that the modulation components $V_{ij}^{(\pm)}$ arise due to a cubic nonlinear term (i.e., $V_{ij}^{(\pm)} \propto V_i V_j V_p$), the individual combinations $V_{ij}^{(\pm)}/(V_i V_j V_p)$ should not depend on the pump amplitudes. However, the above mentioned bad stability of individual coefficients is even worse for the cascade interactions. Therefore, by analogy with coefficient (1) for the conventional modulation, the following cumulative coefficient can be written for cascade components:

$$K_3 = \sqrt{\sum_{i,j} (V_+^2(i,j) + V_-^2(i,j))} \Big/ \left[\left(\sum_{i,j} V_{pm}^2(i) V_{pm}^2(j) \right)^{1/2} V_p \right] \tag{2}$$

For this coefficient much like for coefficient (1), not the absolute, but only the relative values for reference and studied samples have physical meaning.

By analogy with the quadratic character of coefficient (1), a fairly constant value of K_3 under varying amplitudes of interacting waves should be observed for a cubic nonlinearity. In this context, a "non-cubic" behavior of K_3 (e.g., its pronounced dependence on time in the case of gradually decaying impact-excited pump modes) can serve as a signature of a non-analytical character of the sample nonlinearity. This in turn indicates a high probability of the presence of soft structural defects (first of all, cracks or delaminations with clapping contacts).

Some examples of temporal dependences for the coefficients K_2 defined by Eq. (1) are shown in Fig. 6 together with the cascade coefficient K_3. Coefficients K_2 are truly cumulative over all $\omega \pm \Omega_i$ sidelobes that well exceed the noise. However, for clarity, coefficients K_3 in Fig. 6, actually are individual coefficients found for several most intense cascade modulation components and the corresponding generating pump modes. The samples are an axle with a natural transversal crack, a naturally-damaged disk, and another axle with an artificial crack-like defect (the two latter samples are the same as for Fig. 3). In view of exponential character of the pump-field decay, the time axis in Fig. 6 roughly corresponds to the logarithm of the pump-action amplitude (the exact proportionality could be if the decay times were equal for all pump modes).

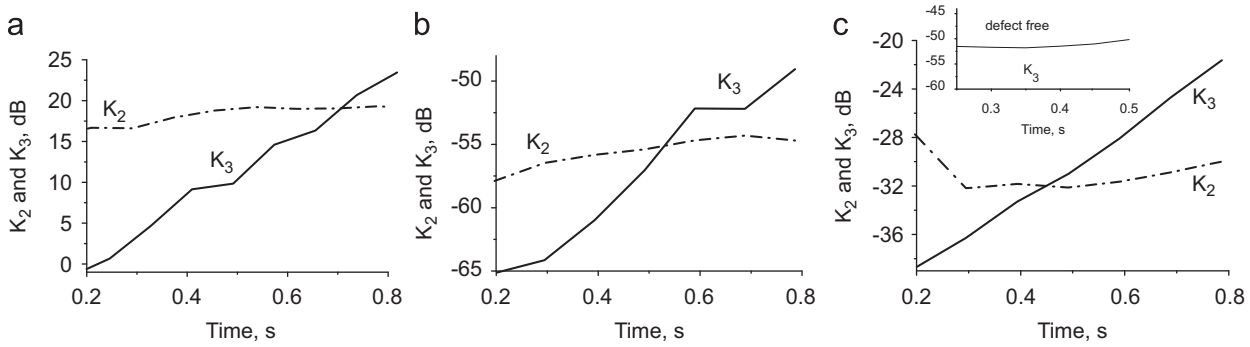

Fig. 6. Time behavior of the cubic-type nonlinear coefficient $K_3 = M_{1+2}/(S_1 S_2 S_p)$ corresponding to selected intense cascade components in the modulation spectra and the cumulative quadratic-type coefficient K_2 defined by Eq. (1) for conventional sidelobes. The time is counted from the moment of the impact excitation of the pump modes. Panel (a) is for the axle with a transversal natural fatigue crack. Panel (b) is for a railway-wheel disk with natural fatigue damage, the same as in Fig. 3. Panel (c) is the axle with an artificial defect in the form of a saw-cut with inserted steel plate (the same as in Fig. 3); the inset shows that without the inserted plate (defect-free case), coefficient K_3 is quite stable and corresponds to non-clapping cubic nonlinearity.

Fig. 6 shows that coefficient K_3 is pronouncedly non-constant unlike fairly stable conventional-modulation coefficient K_2. This fact indicates that the cascade components were predominantly produced by a non-cubic nonlinearity. The inset in the plot c in Fig. 6 (corresponding to the axle with the artificial crack in the form of a saw-cut with an inserted steel plate) shows for comparison the coefficient K_3 in the absence of the defect (the plate removed from the saw-cut). It is seen that in such a defect-free case the coefficient K_3 remains fairly stable as expected for a classical cubic nonlinearity. In contrast, for the samples with crack-like defects, the pronounced increase in K_3 with increasing time (i.e., decreasing pump amplitude) indicates that the cascade sidelobes exhibit a clear trend to saturation at higher pump amplitudes. This observation well agrees with the expectation that the pump modes can be sufficiently intense to cause clapping of inner contacts in the cracks and thus ensure a non-analytical nonlinearity of the crack-like defects.

The latter conclusion, however, apparently contradicts with quite stable values of the above introduced coefficient K_2 for the classical (quadratic) modulation components $\omega \pm \Omega_i$ in exactly the same experimental runs. Fairly stable K_2 apparently leads to the conclusion that even for the samples with cracks, the nonlinearity can be approximated by a power-series with the leading quadratic term. To resolve this paradox, in the next section we consider in more detail the expected amplitude behavior of conventional and cascade modulational sidelobes using a simple model of the defect.

4. Simulations of modulation-sidelobe behavior in the case of multi-frequency pump excitation

For the purpose of the present consideration, it is sufficient to consider functional dependences and relative variations of the sidelobes rather than their absolute estimates. Thus we will not take into account resonant properties of the sample (unlike study [13]), but simply consider the nonlinear source of the corresponding modulational components. Recalling Fig. 2, which demonstrates that the nonlinearity of crack-like defects can be strongly dominated by the Hertz-contact contribution, we will model the nonlinear source by a weakly pre-compressed Hertzian contact that can be transferred into clapping regime by sufficiently intense acoustic excitation. A similar model was used in Ref. [14] in the discussion of cross-modulation phenomena (i.e., the transfer of amplitude modulation from one carrier wave to another one). The weak background nonlinearity of the matrix material in this approach can be modeled by a term corresponding to a much stronger prestrained contact, which cannot be transferred into clapping regime even at maximal pump amplitudes. Actually this second term can always be expanded into power series in strain amplitudes. Thus we consider the following nonlinear function:

$$\sigma_0 + \tilde{\sigma} = A(\varepsilon_0 + \tilde{\varepsilon})^{3/2} H(\varepsilon_0 + \tilde{\varepsilon}) + B(\mu\varepsilon_0 + \tilde{\varepsilon})^{3/2} H(\mu\varepsilon_0 + \tilde{\varepsilon}). \quad (3)$$

Here, like in Ref. [14], $H(\ldots)$ is a Heaviside function indicating that the contacts do not bear a tensile stress; σ_0 and ε_0 are the static stress and the corresponding static strain in the sample, which is needed in the model to adjust the level of the background (i.e., without the defect) nonlinearity; perturbations $\tilde{\varepsilon} << \varepsilon_0$ and $\tilde{\sigma} << \sigma_0$ are the acoustic strain and stress. Small parameter $\mu \ll 1$ in the second term describes the pre-strain of the weak contact (i.e., the defect). Parameters A and B in Eq. (3) allow one to adjust the relative strength of nonlinearity of the defect and the matrix material by varying the ratio B/A.

In view of the condition $\tilde{\varepsilon} << \varepsilon_0$, the Heaviside function can be omitted in the first ("matrix") term of the right-hand side of Eq. (3). In contrast, in the second term describing the defect, the weak pre-strain $\mu\varepsilon_0$ can be comparable with the acoustic strain $\tilde{\varepsilon}$, such that the contact can be transferred into clapping regime for $|\tilde{\varepsilon}| > |\mu\varepsilon_0|$ (note that parameter μ in the general case can also be negative, which corresponds to an initially weakly open contact). For sufficiently small $|\tilde{\varepsilon}| < |\mu\varepsilon_0|$, the second term can be expanded into a power series like the first non-clapping term, such that the dimensionless quadratic nonlinear parameter β in the resultant expansion of the acoustic perturbations $\tilde{\sigma}(\tilde{\varepsilon}) \propto \tilde{\varepsilon} + \beta\tilde{\varepsilon}^2 + \ldots$ can be represented as $\beta \approx (1/2)\varepsilon_0^{-1}[1 + (B/A)\mu^{-1/2}]$.

Typical values on the nonlinear parameter in homogeneous solids can readily be modeled by choosing the corresponding pre-strain ε_0. For example, $\varepsilon_0 = 10^{-1}$ corresponds to the nonlinear quadratic coefficient $\beta \approx \varepsilon_0^{-1}/2 = 5$ related to the first ("matrix") term in the right-hand side of Eq. (3), which is typical for homogeneous metals [11,12]. Then choosing $\mu = 5 \cdot 10^{-5}$ we ensure that the threshold acoustic amplitude $\tilde{\varepsilon} = \mu\varepsilon_0 = 5 \times 10^{-6}$ transfers the weak contact into clapping regime. Further, choosing the ratio $(B/A) = 2\mu^{1/2} \approx 1.41 \times 10^{-2}$ we see that the second term in the right-hand side of Eq. (3) results in the increase of the total value of quadratic nonlinear parameter β by a factor of three (i.e., by about 10 dB) compared with the background initial value $\beta \approx \varepsilon_0^{-1}/2$. For conventional $\omega \pm \Omega$ modulation sidelobes, this increase in β should result in a similar 10 dB increase, which is still comparable with the natural variability of the conventional-modulation level for different samples (as discussed in detail in

Ref. [13]). Therefore such a moderate 10 dB contrast in the level of the conventional-modulation is not yet sufficient for making unambiguous conclusions on the presence or absence of the defect (see the corresponding real examples in Fig. 2).

The next step is to compare the contrast in the level of the next-order (cascade) sidelobes $\omega \pm (\Omega_i \pm \Omega_j)$ arising due to the interaction of a probe wave at frequency ω_p with two pump waves at frequencies $\Omega_{i,j}$. Especially interesting is to consider the transition of the contact to clapping regime. Unlike the simple generation of higher-order harmonics for which identical power law with the 3/2 exponent is expected in the clapping regime (as demonstrated in Fig. 2), the amplitude behavior of the cascade sidelobes can hardly be studied analytically, but can easily be simulated using Eq. (3) and a multi-frequency spectrum of $\tilde{\varepsilon}$. The performed numerical simulations indicate that in this case, not only the ratio of individual wave amplitudes to the clapping threshold strain $\mu\varepsilon_0$ is important, but also the ratio between the amplitudes of the interacting waves themselves. Here we consider a probe excitation S_p and two different pump waves with strain amplitudes S_1 and S_2, which is sufficient to demonstrate the main features of cascade modulation components M_{1+2} around the probe wave at frequencies $\omega_p \pm \Omega_1 \pm \Omega_2$. For comparison we also consider the conventional modulation sidelobes M_1 and M_2 (at frequencies $\omega_p \pm \Omega_1$ and $\omega_p \pm \Omega_2$). In the simulation, the probe-wave amplitude is assumed constant ($S_p = \mu\varepsilon_0/10$), i.e., significantly smaller than the clapping threshold $\mu\varepsilon_0$ to which we assign zero-dB value. To represent the results in a simpler understandable 2D-plot, we ensure that one pump-wave amplitude S_1 is kept constant and the second pump-wave amplitude S_2 varies from sub-threshold to significantly super-threshold amplitudes: $\mu\varepsilon_0/30 < S_2 < 30\mu\varepsilon_0$.

Fig. 7 shows examples of the amplitude dependences for M_2 (the conventional modulation sidelobe induced by the pump-wave S_2 with varying amplitude) and the cascade component M_{1+2} (of the $\omega_p \pm \Omega_1 \pm \Omega_2$ type) in the presence and absence of the weak contact. Its absence corresponds to $B=0$ in Eq. (3). The choice of particular wave frequencies is not very important (they only must be different, better incommensurable to avoid degenerate cases). The plots in Fig. 4a and b correspond to two significantly different interaction regimes.

First, consider the case of small $S_1 = \mu\varepsilon_0/5 < \mu\varepsilon_0$, for which the initial part of the curves in Fig. 7a (where $S_2 < \mu\varepsilon_0$) corresponds to the non-clapping regime of the weak contact, whose nonlinearity can be expanded in a series in powers of strain similar to the classical atomic nonlinearity. Thus for $S_2 < \mu\varepsilon_0$, the sidelobe M_2 is produced by the quadratic term and is proportional to S_2 both in the presence and absence of the contact as is seen in Fig. 7a (curves marked by squares). For larger $S_2 > \mu\varepsilon_0$ corresponding to the contact clapping, Fig. 7a demonstrates that M_2 increases somewhat slower than for the pure quadratic regime, but remains monotonic.

Much stronger is the difference between the before-clapping and clapping regimes for the cascade component M_{1+2}. Its behavior in the before-clapping regime is dominated by the cubic term in the nonlinear-function expansion. Therefore, M_{1+2} is proportional to $S_1 S_2 S_p$ and increases as a linear function of S_2 as is seen in Fig. 7a in the region $S_2 < \mu\varepsilon_0$. However, for $S_2 > \mu\varepsilon_0$, unlike the conventional modulation sidelobe M_2, the behavior of M_{1+2} becomes non-monotonic. Near $S_2 \approx \mu\varepsilon_0$ its amplitude rapidly decreases and passes through zero (which looks like a sharp minimum in the log–log plot in Fig. 7a), then M_{1+2} reaches a smooth maximum and slowly decreases again. The reason of passing through zero is that near $S_2 \approx \mu\varepsilon_0$, the phase of the cascade component switches to the opposite (causing the side-lobe-amplitude compensation). Similar non-monotonic behavior due to clapping Hertzian nonlinearity is known for the third harmonic of initially sinusoidal excitation [20]. In the context of NDT applications, comparing the cases of the presence (filled symbols) and the absence (empty symbols) of the soft contact, one can see the remarkable difference in the contrast of the conventional (squares) and cascade components (triangles; about 10 dB and 60–40 dB, respectively).

In the second example shown in Fig. 7b, the amplitude of the invariable first pump wave significantly exceeds the clapping threshold, $S_1 = 3\mu\varepsilon_0$, whereas the second pump wave S_2 varies in exactly the same range as in Fig. 7a. It is clearly seen in Fig. 7b that despite the essentially clapping nonlinearity of the weak contact, the amplitude M_2 remains linearly proportional to S_2 like for the classical quadratic nonlinearity. More precisely, the simulation shows that the value of M_2 produced by the pump wave S_2 also depends on S_1 for $S_1 \gg \mu\varepsilon_0$, albeit fairly slowly ($\sim S_1^{-1/2}$).

What for the cascade component M_{1+2} (marked by filled triangles in the presence of the clapping weak contact), its behavior changes much stronger compared with Fig. 7a. Namely, the peculiar minimum near $S_2 \sim \mu\varepsilon_0$ disappears and the cascade-component amplitude M_{1+2} remains linearly proportional to amplitude S_2 while $S_2 < S_1$. Then for $S_2 > S_1$, the M_{1+2} component exhibits saturation and even slightly decreases at $S_2 \gg S_1$. In the NDT context, it is important to emphasize that the presence of the clapping weak contact again results in a strong (about 50 dB) increase in the level of the cascade sidelobe M_{1+2}. compared with only $\sim$10 dB increase in the level of the classical sidelobe M_2 as is seen in Fig. 7b.

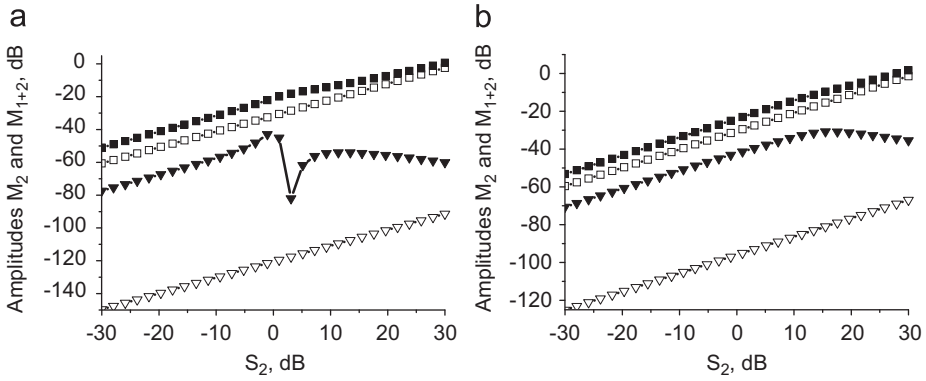

Fig. 7. Simulated amplitude dependences of conventional sidelobes M_2 (squares) and cascade components M_{1+2} (triangles). Filled symbols correspond to the presence and empty symbols, to the absence of the defect. Plot (a) is for the small amplitude of the first pump wave $S_1 = const. = \mu\varepsilon_0/5$, and (b) is for the intense pump wave with amplitude exceeding the clapping threshold, $S_1 = const. = 3\mu\varepsilon_0$. For both plots, the probe-wave amplitude is $S_p = \mu\varepsilon_0/10$ and the second pump-wave amplitude varies in the range $\mu\varepsilon_0/30 < S_2 < 30\mu\varepsilon_0$.

Calculations similar to those illustrated in Figs. 7a and b were performed for various amplitudes of interacting waves and for different exponents (not necessarily Hertzian 3/2) of the clapping nonlinearity. Table 1 shows the results for the so-found scaling laws for conventional sidelobes M_1 and M_2 and cascade M_{1+2}, including the case of the presence of an additional strong excitation $S_0 > S_1$, S_2, S_p and $S_0 > \mu\varepsilon_0$. The table shows, that if among several interacting waves one wave is the most intense and significantly exceeds the clapping threshold, then for all other weaker waves, the clapping nonlinearity is effectively smoothed. Consequently, interactions of the weaker waves exhibit the scaling laws rather typical of classical power-law (quadratic or cubic) nonlinearities, although the values of the effective quadratic and cubic nonlinear parameters are controlled by the strongest wave. For the right column in the table, this strongest excitation is S_0, and for the middle column, this is S_1. Table 1 also shows that the dependence of the effective cubic nonlinear parameter on the strongest-wave amplitude is more pronounced than for the quadratic one.

In particular, for the Hertzian nonlinearity with $n=3/2$, if either pump component S_1 or S_0 is the strongest and exceeds the clapping threshold (i.e., $S_1 \gg \mu\varepsilon_0$ or $S_0 \gg \mu\varepsilon_0$), then the cascade sidelobe scales as $M_{1+2} \propto (S_1S_2S_p)S_{1,0}^{-3/2}$ rather than $M_{1+2} \propto S_1S_2S_p$ expected for the classical cubic nonlinearity. Therefore, for the classical cubic nonlinearity, the ratio $M_{1+2}/(S_1S_2S_p)$ should be constant, whereas for multi-wave interactions due to the clapping Hertzian contacts, the combinations $M_{1+2}/[(S_1S_2S_p)S_{1,0}^{-3/2}]$ should remain constant. We also emphasize that for the conventionally observed sidelobes $M_{1,2}$, the influence of the strongest wave in the clapping regime is much weaker than for the cascade sidelobes. Table 1 indicates that instead of classical quadratic scaling laws $M_1 \propto S_1S_p$ and $M_2 \propto S_2S_p$, the clapping nonlinearity in the presence of the most intense wave $S_1 \gg \mu\varepsilon_0$ or $S_0 \gg \mu\varepsilon_0$ results in the modified scaling laws $M_1 \propto (S_1S_p)S_{1,0}^{-1/2}$ and $M_2 \propto (S_2S_p)S_{1,0}^{-1/2}$. In other words, for the conventional sidelobes M_1 and M_2, the "clapping" scaling law is modified by the most intense wave significantly weaker, by the factor $S_{1,0}^{-1/2}$ instead of factor $S_{1,0}^{-3/2}$ for the cascade sidelobes. It is interesting that in the presence of the most intense "smoothing" wave $S_{1,0} > S_2$, S_p, the proportionality $M_2 \propto S_2S_p$ can persist even if all amplitudes belong to the clapping region, $S_2 \gg \mu\varepsilon_0$ and $S_p \gg \mu\varepsilon_0$.

Now we may return to the above formulated paradox that in the same measurements, the conventional modulational sidelobes $M_{1,2}$ can behave almost like in the classical quadratic case, whereas the cascade components M_{1+2} indicate a quite pronounced non-classical regime of clapping nonlinearity. We recall that normally the strongest impact-excited mode is one of the lowest eigenmodes for which the decay rate is much smaller than for others, so that during the decay time of the higher-order modes, such an intense mode (S_0 or S_1 in Table 1) can decay relatively insignificantly. Therefore, for conventional sidelobes induced by almost all other pump modes, one can expect fairly insignificant difference between the "clapping" scaling and classical quadratic scaling (e.g., $M_2 \propto (S_pS_2)S_{0,1}^{-1/2}$ and $M_2 \propto S_pS_2$, respectively). In addition, the atomic nonlinearity can also give a non-negligible contribution to the conventional sidelobes, such that their resultant behavior can demonstrate even weaker dependence on the strongest-wave amplitude than scaling $S_{0,1}^{-1/2}$ expected for the pure clapping.

In contrast, for the cascade component M_{1+2}, the background contribution of the atomic nonlinearity is orders of magnitude smaller, whereas the clapping nonlinearity results in a significantly steeper $S_{0,1}^{-3/2}$ dependence on the amplitude of the strongest wave. These conclusions explain the apparent contradiction between the simultaneously observed almost quadratic classical scaling law for conventional sidelobes $\omega \pm \Omega_i$ and pronounced deviation from classical cubic scaling for cascade sidelobes $\omega \pm \Omega_i \pm \Omega_j$. In the NDT context, this pronounced functional difference of the cascade-sidelobes scaling from the classical cubic law can be used as an additional signature of the presence of crack-like defects in the sample.

5. Comparison of experimental data with the simulated scaling laws for clapping contacts

We have already seen from Fig. 6 that in the discussed experiments with impact-excited multiple pump modes, the cascade components demonstrate significant deviation from the classical cubic scaling, since the ratio $M_{1+2}/S_1S_2S_p$ does not remain constant as a function of time. This fact indicates a non-analytical regime of the defect's nonlinearity. According to the performed simulation, this can be ensured if at least one of the pump modes (which we denote S_0) has amplitude $S_0 \gg \mu\varepsilon_0$.

Let us discuss in more detail the sample (railway axle) with a natural transversal crack, the same as for Fig. 6a. The examination of the spectrum of impact-excited modes confirmed the expectation that the lowest most intense modes had minimal decay rates. One of those modes (903 Hz) was identified as the lowest longitudinal mode. The accelerometer aligned with the axle axis indicated that the initial strain amplitude for this mode exceeded 10^{-5}. Further examination showed that there was another, obviously non-longitudinal and fairly intense mode at 190 Hz. The vibrations for this mode should be orthogonal to the axis and thus could be registered only due to parasite transversal sensitivity of the accelerometer. Thus the actual stain amplitude for this mode could strongly exceed the apparent value. It was naturally to assume that this intense and slowly decaying mode at 190 Hz could ensure the clapping regime of the defect (i.e., it could play the role of modes S_1 or S_0 in Table 1). It is essential that for the discussion of the functional behavior of the sidelobes we do not need to know the exact amplitude of this most intense mode.

According to the previous section one may expect that, for the conventional modulation, the own sidelobe of the strongest mode S_0 could demonstrate the most clear scaling of the type $\propto S_pS_0^{1/2}$, whereas for other modes, the classical quadratic scaling $M_j \propto S_pS_j$ could be corrected by the strongest mode resulting in the "clapping" scaling law $M_j \propto (S_pS_j)S_0^{-1/2}$. Fig. 8 shows the corresponding examples for several conventional sidelobes, which well agree with such expectations. The sample is the railway axle with a natural crack (the same as for Fig. 6a).

Since the modes decay nearly exponentially, in the logarithmic scale, the horizontal time axis in Fig. 8 is proportional to the

Table 1
Scaling laws for the modulational sidelobes in clapping and non-clapping regimes.

	$S_1+S_2+S_p < \mu\varepsilon_0$	$S_1 \gg \mu\varepsilon_0$ and $S_1 > S_p, S_2$	$S_0 \gg \mu\varepsilon_0$ and $S_0 > S_p, S_1, S_2$
M_1	S_pS_1 (and does not depend on S_2)	$S_pS_1^{n-1} = (S_pS_1)S_1^{n-2}$	$(S_pS_1)S_0^{n-2}$
M_2	S_pS_2 (and does not depend on S_1)	$(S_pS_2)S_1^{n-2}$	$(S_pS_2)S_0^{n-2}$
M_{1+2}	$S_pS_1S_2$	$S_pS_2S_1^{n-2} \equiv (S_pS_2S_1)S_1^{n-3}$	$(S_pS_2S_1)S_0^{n-3}$

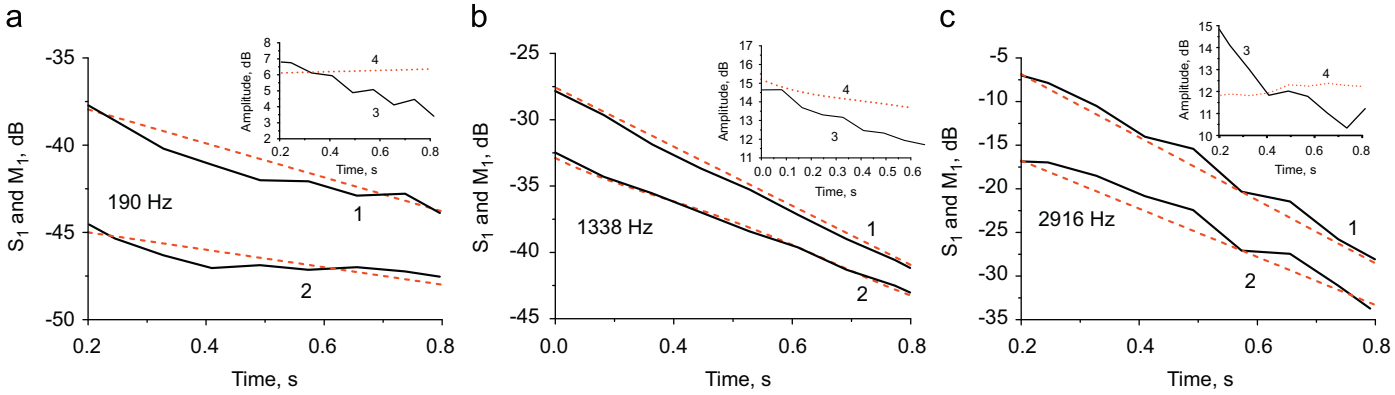

Fig. 8. Examples of time dependences for intense pump modes S_1 (lines marked 1) and the corresponding conventional modulation sidelobes M_1 (lines marked 2) in the railway axle with a natural transversal crack. Dashed lines show the averaged slopes. The insets show clearly decreasing ratios S_1/M_1 (lines marked 3) and fairly stable smoothed clapping-type scaling coefficients $M_1 S_0^{1/2}/S_1$ (lines marked 4). For all panels, the most intense pump wave S_0 corresponds to the 190 Hz mode, such that $S_1 = S_0$ for panel (a).

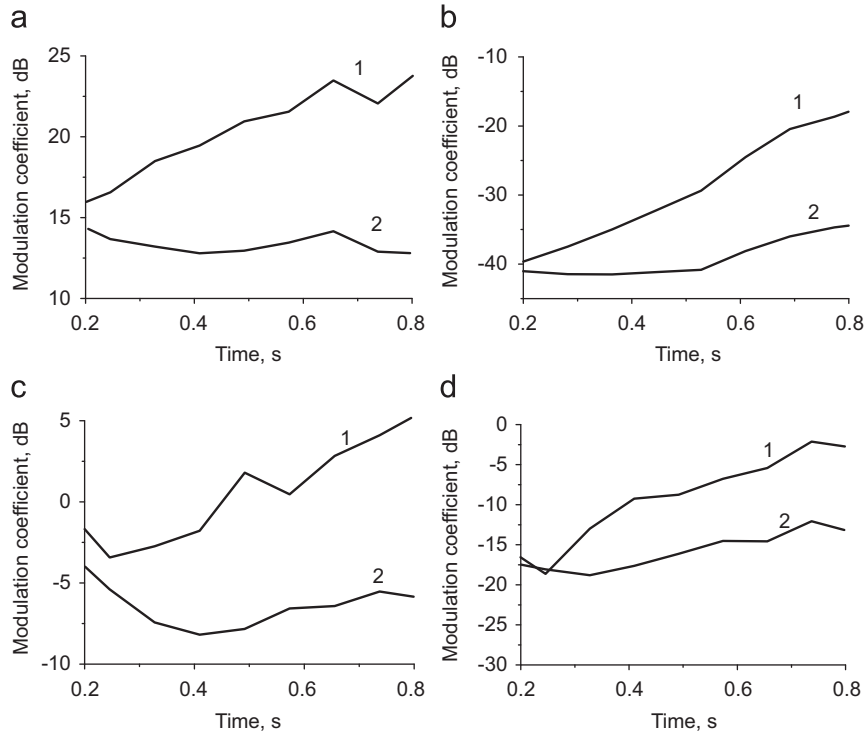

Fig. 9. Examples of pronouncedly growing with time cubic-type cascade coefficient (4) (curves marked 1) and clapping-type cascade coefficient (5) exhibiting much stabler values (curves marked 2). Panel (a) and (b) are for degenerate modulational sidelobes separated from the probe-wave frequency by the double pump-wave frequency 190 Hz+190 Hz and 2916 Hz+2916 Hz, respectively. Panels (c) and (d) are for non-degenerate sidelobes corresponding to the interaction of different pump modes (903 Hz+1338 Hz and 903 Hz+2916 Hz, respectively).

amplitude of the respective wave. Thus for classical quadratic-type scaling $M_i \propto S_i S_p$, the time dependences of the pump-modes S_i and their modulational sidelobes M_i should look as parallel lines. However, Fig. 8 demonstrates that the sidelobes actually decay slower. The averaged slopes for the pump modes and the respective sidelobes indicate that, for the pump mode at 190 Hz, the sidelobe scales closely to $\propto S_0^{1/2}$, whereas for the other modes at 1338 and 2916 Hz, the ratios of the slopes are close to $\propto S_0^{0.75}$, which also fairly well agree with the above discussed scaling laws for clapping contacts. The insets in Fig. 8 additionally show the ratios M_i/S_i, which are clearly decreasing in contrast to values $M_i S_0^{1/2}/S_i$, which are fairly stable as expected for the contact-clapping regime (see Table 1).

Let us now discuss the scaling behavior of cascade sidelobes for the same sample. First, we consider the coefficient of the cubic type

$$K_3^{cub} = \frac{M_{1+2}}{S_p S_1 S_2}, \tag{4}$$

which should remain constant if the cascade components M_{1+2} were produced by the pump modes S_1 and S_2 that interact with the probe wave S_p due to cubic classical nonlinearity. The modified coefficient of the form

$$K_3^{clap}(S_0 > S_1) = \frac{M_{1+2}}{S_p S_1 S_2} S_0^{3/2}, \tag{5}$$

should remain constant if the interaction is due to the clapping Hertzian nonlinearity and the strongest wave S_0 does not directly participate in the generation of the sidelobe M_{1+2} (see the right column in Table 1 for $n=3/2$). If the strongest mode directly participates in the interaction (which corresponds to the case $S_1=S_0$), the "clapping" coefficient takes the form

$$K_3^{clap}(S_0=S_1)=\frac{M_{0+2}}{S_pS_2}S_0^{1/2} \tag{5'}$$

Examples of time dependences for coefficients (4), (5) and (5′) are shown in Fig. 9. Panels (a) and (b) in Fig. 9 are for the degenerated cascade components corresponding to the double frequency of the pump modes at 190 and 2916 Hz, respectively. Panels (c) and (d) are for the non-degenerated cascade sidelobes produced by combined action of the pump modes (903 Hz+1338 Hz) and (903 Hz+2916 Hz), respectively. In the calculation of the modified coefficient K_3^{clap}, in all cases the 190 Hz mode is considered the strongest. All examples show that coefficient K_3^{cub} corresponding to the cubic scaling defined by Eq. (4) is non-constant (pronouncedly growing with the time), whereas the modified clapping-type coefficients K_3^{clap} defined by Eqs. (5) and (5′) remain fairly stable. Therefore, the scaling expected for the clapping nonlinearity much better describes the actual behavior of the cascade sidelobes and confirms the expectation that the change in the scaling law due to clapping is much more pronounced for cascade sidelobes than for the conventionally observed lower-order sidelobes.

In conclusion, Fig. 10 shows the same experimental data as for Fig. 9d (but in a wider time range) together with the simulated values of the cascade coefficients. The simulation was made using Eq. (3) in which we substituted the amplitudes S_0, S_1, and S_2 corresponding to the experimentally observed time dependences for the most intense mode S_0 at 190 Hz and the two other interacting longitudinal modes $S_{1,2}$ at 903 and 2916 Hz. The cubic-type cascade coefficient (4) was used to calculate curve 1′ in Fig. 10, whereas curve 2′ is for the clapping-type coefficient (5). In the modeling, conditions $S_0 \gg \mu\varepsilon_0$ and $S_0 > S_{1,2}$, S_p were the key

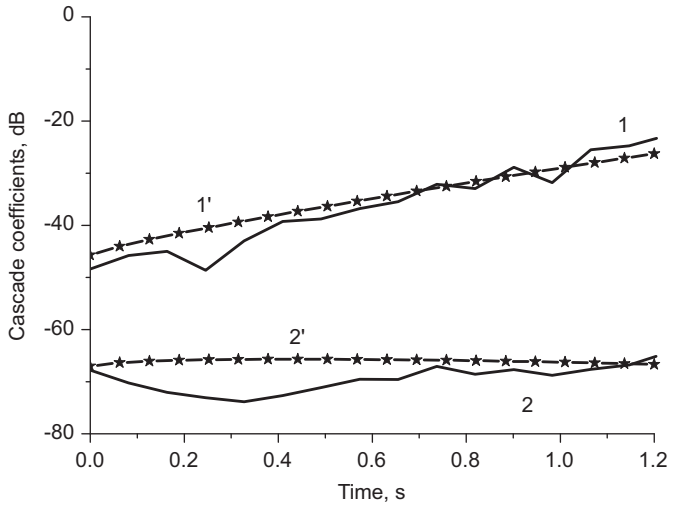

Fig. 10. Cubic-type (curves 1 and 1') and clapping-type (curves 2 and 2′) cascade coefficients for the cascade modulation sidelobe generated by the pump modes at 903 and 2916 Hz. Solid curves correspond to the experiment and curves with asterisks are simulated using Eq. (3). In the simulation, the time dependences of the pump modes were taken from the measurements and the strongest mode at 190 Hz was supposed to be higher in amplitude than the clapping threshold and the other interacting modes. The calculated curves are arbitrarily shifted vertically and superposed with the experimental ones.

assumptions, which ensured fairly good agreement with the observed behavior of the cascade coefficients. That is, it was not necessary to know exact amplitudes of the weaker waves $S_{1,2}$ and S_p since the scaling laws were controlled by the most intense mode that produced the clapping (see Table 1). Since only the functional behavior of the discussed coefficients has physical sense, the calculated curves can be arbitrarily shifted vertically. The superposed simulated and experimental dependences in Fig. 10 demonstrate fairly good agreement. Overall, the scaling laws for the examined modulation sidelobes consistently indicate that the most intense pump wave ensured the clapping regime of the nonlinearity of the crack.

Although the pump-mode amplitudes could be estimated only approximately, the pump-strain amplitudes could hardly exceed 10^{-6}–10^{-5} during most part of the analyzed time window (typically 0.1–1.0 s after the impact). It does not look probable that such moderate strains could close and open the entire crack, because it is known that the strain required to completely close a crack is approximately equal to the ratio of the crack opening to its diameter (crack's aspect ratio). The aspect ratios of about 10^{-6} and less indeed look unrealistically small for cracks. However, it should be taken into account that real cracks' interfaces typically have wavy asperities, which create (or maybe nearly create) inner wavy-shape contacts. At such contacts, locally the separation of the crack surfaces is much smaller (down to nanometer scale) than the average crack opening. Such contacts can already exhibit clapping-type behavior under the influence of strains that are 2–3 orders of magnitude smaller than the strain required to cause clapping of the entire crack. This conclusion is also supported by other experimental data [21,22], so that it is not surprising that strains on the order of 10^{-6} in the discussed experiment could cause clapping of inner crack contacts. We can recall Fig. 2 in which the parallel dependences for different-order higher harmonics clearly indicated clapping regime of Hertzian contacts in the artificial crack-like defect for strains $\sim 10^{-6}$

From the viewpoint of diagnostic applications, it is important to emphasize that the expected contrast in the level of cascade components between damaged and reference samples can be much higher than for the conventional modulation sidelobes normally used in the nonlinear-modulation approach to crack detection (compare the contrasts of 40–60 dB for the cascade components against 5–10 dB for the conventional ones as shown in Fig. 7). On the other hand it should be clearly understood that such a high expected sensitivity of the cascade components is much more demanding to the linearity of the entire measurement system. Unlike the conventional modulation for the cascade sidelobes, the main masking factors are additive noises, technical nonlinearities in the measurement equipment and, especially, the nonlinearity of the supporting system rather than the background atomic nonlinearity.

The experimental spectra (a) and (a′) in Fig. 3 demonstrate that the parasite nonlinearity of the measurement system produces quite a noticeable level of cascade component even for reference defect-free samples. This did not allow us to attain the 40–60 dB contrast expected if the cascade sidelobes were produced by the atomic nonlinearity. Nevertheless, even in real experiments the contrast in the cascade modulation between the reference and damaged samples is much better than for conventional modulation.

6. Conclusion

To conclude we emphasize the main points discussed in this article.

- The performed study was motivated by the earlier obtained conclusion [13] that for the presently achieved quality of measurements, it is the atomic nonlinearity which limits the ultimate sensitivity of the conventional nonlinear-modulation method of crack detection based on the use of quadratic-type nonlinear interactions.
- A natural way to further improve the sensitivity of the nonlinear-modulation approach can be the use of more complex (higher-order) modulational interactions, for which the background contribution of the atomic nonlinearity should be drastically reduced. In the present study, we focused on the modulational components of the $\omega \pm \Omega_i \pm \Omega_j$ type, which naturally appear in schemes with impact-excited multi-frequency pump excitation like in Ref. [13–15]. For such cascade components, the background atomic nonlinearity should contribute via cubic terms, whose intensity is negligibly small. It is experimentally shown that reliable observation of crack-produced cascade modulation is possible despite the parasite nonlinearities of the measurement system, whose masking influence becomes the main limiting factor. It is demonstrated that the energy of the higher-order modulation sidelobes $\omega \pm \Omega_i \pm \Omega_j$ can ensure significantly higher contrast between reference and damaged samples compared with the energy of the conventionally observed sidelobes $\omega \pm \Omega_i$ (see the examples in Figs. 3–5).
- The performed simulations and comparison with experiments have lead to the conclusion that the cascade modulational components in samples with crack-like defects can be well described by the clapping Hertzian nonlinearity. The modeling explained why even for clapping Hertzian nonlinearity of inner contacts in cracks, the behavior of conventional modulational components of the $\omega \pm \Omega$ type can be reasonably well approximated assuming the simplest classical quadratic nonlinearity of the contacts. This effect of "smoothed" clapping nonlinearity can be compared with the well-known "smoothing" of the dry friction by an intense high-frequency wave, which produces effective viscous-like damping (the dithering effect).
- For the cascade components $\omega \pm \Omega_i \pm \Omega_j$, the clapping character of the nonlinearity is more important and results in pronouncedly non-cubic-type scaling laws. In the NDT context, this functional difference between the modulational sidelobes generated due to classical power-law and clapping nonlinearities can also be used to detect the presence of nearly closed cracks, as well as such defects as delaminations or damaged adhesive connections, for which similar contact-type nonlinearities are also typical [23,24].

Overall, it can be concluded that cascade-modulation effects can be of practical interest to improve the sensitivity of the nonlinear-modulation approach to crack detection, although this approach is much more demanding to the linearity of the entire measurement system.

Acknowledgement

The study was supported by the RFBR Grant no. 08-02-97039-r and the French-Russian PICS project co-funded by RFBF and CNRS (Grant no. 09-02-91071).

References

[1] Ekimov AE, Didenkulov IN, Kazakov VV. Modulation of torsional waves in a rod with a crack. J Acoust Soc Am 1999;106(3–1):1289.
[2] Johnson P. The new wave in acoustic testing. Materials world. J Inst Mater 1999;7:544.
[3] Zaitsev VYu, Sas P. Nonlinear response of a weakly damaged metal sample: a dissipative mechanism of vibro-acoustic interaction. J Vib Control 2000;6:803–22.
[4] Van Den Abeele KEA, Sutin A, Carmeliet J, Johnson P. Microdamage diagnostics using nonlinear wave spectroscopy (NEWS). NDT&E Int 2001;34:239–48.
[5] Donskoy D, Sutin A, Ekimov A. Nonlinear acoustic interaction on contact interfaces and its use for nondestructive testing. NDT&E Int 2001;34:231–8.
[6] Solodov I, Wackerl J, Pfleiderer K, Busse G. Nonlinear self-modulation and subharmonic acoustic spectroscopy for damage detection and location. Appl Phys Lett 2004;84:5386.
[7] Sutin AM, Johnson PA Nonlinear elastic wave NDE II. Nonlinear wave modulation spectroscopy and nonlinear time reversed acoustics. In: Proceedings of 31st annual review of progress in QNDE. Proceedings of AIP conference, vol.760, 2005. p.385–92.
[8] Rudenko OV. Giant nonlinearities in structurally inhomogeneous media and the fundamentals of nonlinear acoustic diagnostic techniques. Phys-Usp 2006;49:69–87.
[9] Duffour P, Morbidini M, Cawley P. A study of the vibro-acoustic modulation technique for the detection of cracks in metals. J Acoust Soc Am 2006;119(3):1463–75.
[10] Straka L, Yu Yagodzinskyy, Landa M, Hanninen H. Detection of structural damage of aluminium alloy 6082 using elastic wave modulation spectroscopy. NDT&ElInt 2008;41:554–63.
[11] Zarembo LK, Krasilnikov VA. Nonlinear phenomena in the elastic wave propagation in solids. Sov Phys Usp 1971;13:778.
[12] Kittel C. Introduction to solid state physics. 7th ed.. New York: Wiley; 1996.
[13] Zaitsev VYu, Matveev LA, Matveyev AL. On the ultimate sensitivity of nonlinear-modulation method of crack detection. NDT&E Int 2009;42:622–9.
[14] Zaitsev VYu, Matveev LA, Matveyev AL, Arnold W. Cascade cross modulation due to the nonlinear interaction of elastic waves in samples with cracks. Acoust Phys 2008;54(3):398–406.
[15] Matveyev AL, Nazarov VE, VYu Zaitsev, Potapov AI, Erilin ES, Sorokin SV, et al. Nonlinear acoustic method of crack detection in railway wheel pairs. World of nondestructive testing 2004;4(26):65–8. [in Russian].
[16] Zaitsev VYu. A model of anomalous acoustic nonlinearity of micro-inhomogeneous media. Acoust Lett 1996;19(9):171–6.
[17] Belyaeva IYu, Zaitsev VYu. Nonlinear elastic properties of microinhomogeneous hierarchically structured media. Acoust Phys 1997;43(5):510–5.
[18] Fillinger L, Zaitsev V, Gusev V, Castagnède B. Wave self-modulation in an acoustic resonator due to self-induced transparency. Europhys Lett 2006;76(2):229–35.
[19] Courtney CR, Drinkwater BW, Neild SA, Wilcox PD. Factors affecting the ultrasonic intermodulation crack detection technique using bispectral analysis. NDT&E Int 2008;41(3):223–34.
[20] Zaitsev VYu. Nonideally packed granular media: numerical modeling of elastic nonlinear properties. Acoust Phys 1995;41(3):385–91.
[21] Zaitsev V, Gusev V, Castagnede B. Luxemburg–Gorky effect retooled for elastic waves: a mechanism and experimental evidence. Phys Rev Lett 2002;89:105502.
[22] Zaitsev V, Gusev V, Castagnede B. Thermoelastic mechanism for logarithmic slow dynamics and memory in elastic wave interaction with individual cracks. Phys Rev Lett 2003;90:075501.
[23] Solodov IY. Ultrasonics of non-linear contacts: propagation, reflection and NDE-applications. Ultrasonics 1998;36(1–5):383–90.
[24] Yan D, Drinkwater BW, Neild SA. Measurement of the ultrasonic nonlinearity of kissing bonds in adhesive joints. ND&E Int 2009;42(5):459–66.